Geoderma 401 (2021) 115337

Contents lists available at ScienceDirect

Geoderma

journal homepage: www.elsevier.com/locate/geoderma

How the composition of sandstone matrices affects rates of soil formation

D.L. Evans [a,b,*], J.N. Quinton [a], A.M. Tye [c], Á. Rodés [d], J.C. Rushton [c], J.A.C. Davies [a], S. M. Mudd [e]

[a] Lancaster Environment Centre, Lancaster University, Lancaster, Lancashire, UK
[b] School of Water, Energy and Environment, Cranfield University, Cranfield, Bedfordshire, UK
[c] British Geological Survey, Keyworth, Nottinghamshire, UK
[d] Scottish Universities Environmental Research Centre, East Kilbride, UK
[e] School of GeoSciences, University of Edinburgh, Edinburgh, UK

ARTICLE INFO

Handling Editor: Karen Vancampenhout

Keywords:
Soil formation
Soil production
Weathering
Sandstone
Cosmogenic radionuclide analysis
Saprolite

ABSTRACT

Soils deliver multiple ecosystem services and their long-term sustainability is fundamentally controlled by the rates at which they form and erode. Our knowledge and understanding of soil formation is not commensurate with that of soil erosion, in part due to the difficulty of measuring the former. However, developments in cosmogenic radionuclide accumulation models have enabled soil scientists to more accurately constrain the rates at which soils form from bedrock. To date, all three major rock types – igneous, sedimentary and metamorphic lithologies – have been examined in such work. Soil formation rates have been measured and compared between these rock types, but the impact of rock characteristics on soil formation rates, such as rock matrices and mineralogy, have seldom been explored. In this UK-based study, we used cosmogenic radionuclide analysis to investigate whether the lithological variability of sandstone governs pedogenesis. Soil formation rates were measured on two arable hillslopes at Woburn and Hilton, which are underlain by different types of arenite sandstone. Rates were faster at Woburn, and we suggest that this is due to the fact that the Woburn sandstone formation is less cemented that that at Hilton. Similarly, rates at Woburn and Hilton were found to be faster than those measured at two other sandstone-based sites in the UK, and faster than those compiled in a global inventory of cosmogenic studies on sandstone-based soils. We suggest that the cementing agents present in matrix-abundant wackes studied previously may afford these sandstones greater structural integrity and resistance to weathering. This work points to the importance of factoring bedrock matrices into our understanding of soil formation rates, and the biogeochemical cycles these underpin.

1. Introduction

Soils are critical global resources. They are key to our food, water and energy security, mitigating and adapting to climate change, the safeguarding of biodiversity, and the protection of human health (Blum, 2005; McBratney et al., 2014; Adhikari and Hartemink, 2016). Conserving soils so that we meet present-day demands, and those of future generations, is therefore a societal priority (Pimentel et al., 1995). This is especially important in the context of the rising demands from a growing population and widespread soil degradation (Quinton et al., 2010; FAO, 2015; Baude et al., 2019).

A fundamental component of our efforts to ensure the long-term sustainability of the soil resource is a better understanding of the controls on soil thickness. The thickness of a soil is determined by the balance between the rates of soil erosion and those of soil formation. In this paper, we define "soil formation" as the process by which bedrock material is converted into soil (Targulian and Krasilnikov, 2007; Egli et al., 2014; Evans et al., 2019, 2020a). Where rates of soil erosion exceed those of soil formation, the soil profile thins and, as a result, the capacity of the soil to store water, carbon and nutrients is reduced (Evans et al., 2020b). Efforts to ameliorate soil erosion have been, and continue to be, prominent in soil science (Panagos et al., 2015). However, significant knowledge gaps remain in our understanding of the rates of soil formation.

The factors that govern soil formation were conceived in the initial development of soil science (Dokuchaev, 1879; Jenny, 1941; Simonson, 1997). The five factors, namely *Climate, Organisms, Relief, Parent Material* and *Time* have since been employed as a framework upon which to

* Corresponding author at: School of Water, Energy and Environment, Cranfield University, Cranfield, Bedfordshire MK43 0AL, UK.
E-mail address: Daniel.L.Evans@cranfield.ac.uk (D.L. Evans).

https://doi.org/10.1016/j.geoderma.2021.115337
Received 23 October 2020; Received in revised form 25 June 2021; Accepted 1 July 2021
Available online 10 July 2021

base further enquiry into the controls of pedogenesis. Although much of this work is theoretical, there has been a greater effort to empirically measure the rates of soil formation in recent decades (Stockmann et al., 2014). In particular, the innovation and application of terrestrial cosmogenic radionuclide analysis in a range of landscapes (Heimsath et al., 1997; Minasny et al., 2015) has improved the precision of soil formation rates. Some authors have compiled global datasets inventorying cosmogenically-derived rates of soil formation in order to investigate the relationship between climate and pedogenesis (Montgomery, 2007; Portenga and Bierman, 2011). However, decadal to centennial fluctuations in regional and global climatic regimes are unlikely to be detected by cosmogenic radionuclide analysis which determine long-term soil formation rates over 1–100 kyr timescales (Cockburn and Summerfield, 2004).

A more apposite use of terrestrial radionuclide data is to study the control of lithology on soil formation rates, but such work to date has only focussed on comparisons between major rock types such as igneous, sedimentary and metamorphic (Stockmann et al., 2014). One of the largest global *meta*-data analyses of soil formation rates conducted by Portenga and Bierman (2011) specifically omits soil-mantled bedrock, and instead focuses on bedrock outcrops and basin sediments. Nevertheless, the authors found that sedimentary lithologies weather faster than igneous and metamorphic lithologies. This finding is also supported by Morel et al. (2003) in a study comparing soil formation rates from sedimentary (sandstone river bedload) and igneous (granite river bedload) lithologies, and Palumbo et al. (2009) in a similar study between sedimentary (Cretaceous stream sediments) and metamorphic (low grade metamorphosed Palaeozoic rocks) lithologies.

Rocks have an array of physical and geochemical properties, all of which may play different roles in influencing soil formation rates. By studying soil formation across the three major rock types, which are lithologically dissimilar in multiple properties, it is difficult to identify whether there is one lithological property that has a more significant role in pedogenesis. One of the solutions to this is to measure and compare soil formation rates on variations of one lithology, thus limiting the number of lithological properties that may potentially differ.

To the best of our knowledge, few studies have assessed the variability of soil formation rates across one lithology. However, where work has been conducted, it has largely focussed on the effects of grain size on weathering rates. A key concept here is 'percolation theory' which suggests that rates of chemical weathering are principally limited by factors that affect solute transport through heterogeneous media, in this case, the bedrock (Hunt and Ghanbarian, 2016). One of the key factors often emphasised here is the infiltration rate; a factor which is, itself, governed by grain size. Some workers have tested the extent to which percolation theory can be used to predict soil formation and soil depth. For example, Egli et al. (2018) amassed empirical data from alpine and Mediterranean sites, and reported that the model performed well. However, the relationship between grain size and soil formation rates has not always been found. Gontier et al. (2015) used U- and Th-series nuclides to demonstrate that differences in the grain size of granites do not significantly affect the rates of soil formation. This is contrary to the work of Wakatsuki et al. (2005) who showed that soil formation rates in coarser grained granites were significantly faster than those of finer grained granites. The authors proposed that coarser grained minerals in granite have a smaller specific surface area, meaning a smaller volume of water is necessary for weathering than that required by finer grained minerals.

However, rates of soil formation may be regulated by other lithological properties, such as the presence, volume and composition of the interstitial matrix. Non-soluble cements like quartz and K-feldspar overgrowths are able to hold the framework grains of bedrock together and increase their resistance to physical weathering processes. In addition, pore-filling clays can clog pore throats (Tye et al., 2012), reducing the transmission and storage of water, oxidants and acids which could otherwise induce chemical weathering reactions, as suggested by the percolation theory, aforementioned (Hunt and Ghanbarian, 2016). Few studies have explored the influence of interstitial matrices on rates of soil formation, representing a significant knowledge gap.

In this study, we use cosmogenic radionuclide analysis for the first time to investigate the extent to which the lithological variability and, in particular, the nature of the interstitial matrices of sandstone, governs rates of soil formation. We present ^{10}Be-derived soil formation rates for two arable hillslopes in the UK, underlain by a fluvial- and a marine-derived sandstone. Furthermore, we place these rates in the context of those previously measured at two other sandstone-based sites in the UK, and with those measured in similar climatic settings around the world.

2. Materials and methods

2.1. Description of sites

Two catena sequences in England were selected in Autumn 2018 (Table 1; Fig. 1). The first site is a south-west facing hillslope at the Hilton Experimental Site (hereafter, Hilton), situated west of Wolverhampton, in Shropshire (52°33′16.34″ N, 2°19′43.17″ W). This is a long-term study site established in 1976, predominantly to facilitate empirical measurements of soil erosion, but it has been employed in a range of multidisciplinary studies (Reed, 1979; Fullen, 1985, 1992). The second site is a south-facing hillslope at Woburn Experimental Farm (hereafter, Woburn), situated south-west of Bedford in Bedfordshire (52°0′50.73″ N, 0°35′5.63″ W). Woburn was established in 1876 partly as an expansion on to the nearby, long-term experimental farms at Rothamsted (Catt et al., 1975). Hilton and Woburn sit in a temperate oceanic climate (Cfb) between 58–64 m a.s.l and 97–109 m a.s.l., respectively. The mean annual precipitation and temperature is 751 mm and 9.8 °C at Hilton, and 657.4 mm and 9.9 °C at Woburn.

At Hilton, the Sherwood Sandstone Group (Helsby Sandstone formation) has been described as reddish brown, well-cemented, sometimes pebbly, fine to medium grained, sub-angular to sub-rounded and locally micaceous (Bloomfield et al., 2006). The reddish brown colour has been previously described as that of hematite veneers coating the grains (Strong, 1993). Studies on the interstitial matrices of the Helsby Sandstone formation have observed zones of calcite and non-ferroan dolomite cement in some closed or restricted pore spaces, as well as

Table 1
Locational context of the Hilton and Woburn study sites.

		Hilton	Woburn
Locational context	**UK county**	Shropshire	Bedfordshire
	GPS co-ordinates	52°33′16.34″ N, 2°19′43.17″ W	52°0′50.73″ N, 0°35′5.63″ W
	Aspect	South-west	South
	Elevation (m a.s.l)	58–64	97–109
	MAP (mm)	751	657
	MAT (•C)	9.8	9.9
Lithology	**Parent material**	Helsby Formation, Sherwood Sandstone	Woburn Formation, Lower Greensand
	Provenance	Fluvial/aeolian	Marine
	Matrix composition	Detrital mica, precipitated illite–smectite, and authigenic clays.	Nearly matrix-free and uncemented. Negligible clay content (0.1%).
	Porosity (%)	~ 6 – 27	~ 35
Glacial history	**Anglian**	Glaciated	Glaciated
	Last Glacial Maximum	Periglacial conditions	Periglacial conditions
Land-use history	**Forest clearance**	2000 BCE	1000 BCE
	Cultivation	Pastoral farming from 1883	From approx. 1000 BCE
	Current land-use	Grass/shrub cover	Winter cereals

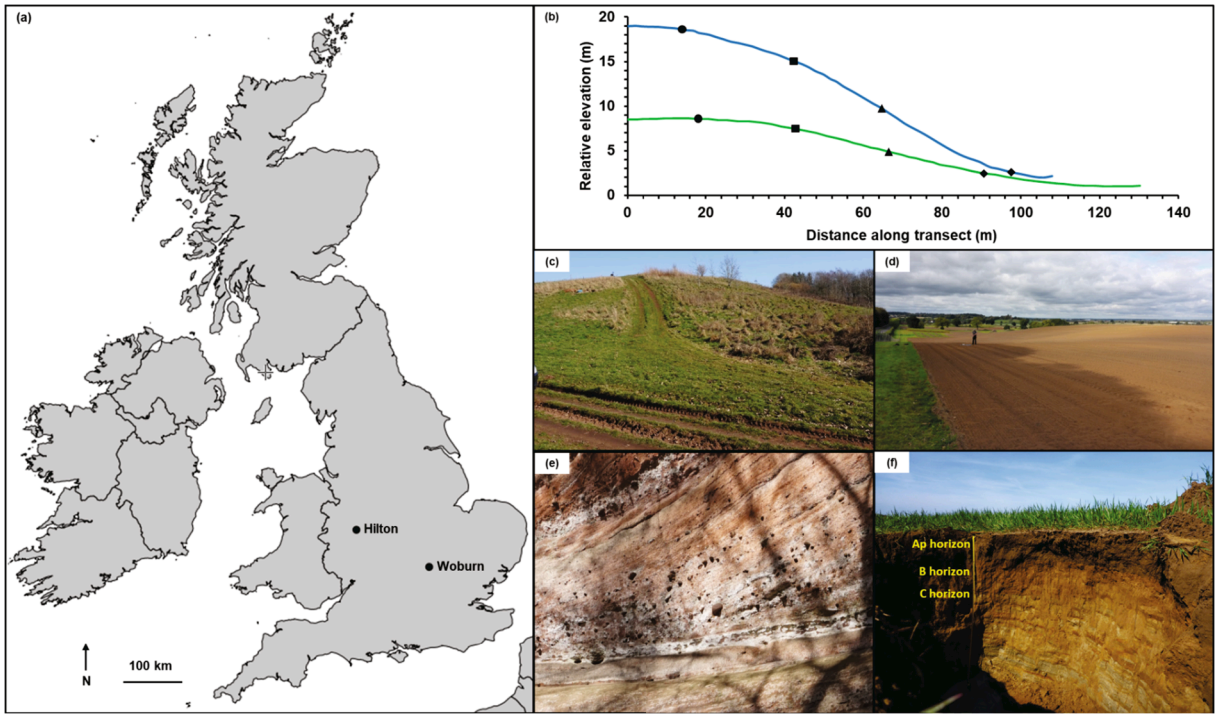

Fig. 1. Location of the study sites (a) with elevation profiles (b) for Hilton (blue) and Woburn (green). Summit (circles), shoulder (squares), backslope (triangles) and toeslope (diamonds) are indicated on each profile. Photographs of the hillslope at Hilton (c) and Woburn (d) were taken from the toeslope during the reconnaissance survey. An exposure of the fluvially-derived sandstone (interbedded with sub-rounded pebbles) close to the study slope at Hilton is shown in (e) (photograph by Miroslav Bauer, 2019). The soil profile, soil-saprolite interface and underlying bedrock at Woburn are shown in (f).

cementation by evaporitic cements such as gypsum, anhydrite, and halite (Strong, 1993; Bloomfield et al., 2006). This cementation most likely represents one of the first stages of the paragenetic sequence in the Helsby sandstone. Evaporitic cements would have been subsequently dissolved, leaving remnants of calcite and non-ferroan dolomites, which are observable today, especially in deeper sections of the bedrock. Studies have also observed evidence of ferroan dolomite, detrital mica, and authigenic illite and kaolinite clay cements in the matrix, representing later stages in the paragenetic sequence. These cements may account for between 30 and 50% of the rock's volume (Burley, 1984; Strong, 1993). This has the effect of reducing porosities to 15% in places.

The provenance of the Helsby Sandstone formation is debated in the literature. Bloomfield et al. (2006) suggest that the formation is predominately fluvial due to the presence of scoured channel bases and rounded mud-clasts. However, these rounded clasts may be the product of reworked aeolian deposits (Mountney and Thompson, 2002). Observations made by the authors suggest that the sandstone at Hilton is predominantly of fluvial origin based on the presence and abundance of sub-rounded to rounded pebbles within the sandstone matrices (Fig. 2a). What is more widely accepted is the fact that the Helsby sandstone formation developed during the Triassic period, when sediments were laid down in desert basins, in dry (~ <300 mm y^{-1}) and hot conditions (Benton et al., 2002). Moreover, previous research has demonstrated that the diagenetic features exhibited in the Sherwood Sandstone group are similar to those in sandstones that form today in the Sonoran Desert (Walker et al., 1978).

At Woburn, the Lower Greensand Group (Woburn Sands formation) has been described as fine to coarse grained, friable rounded quartzose sand (94%) with subsidiary alkali feldspar (2%), glauconite (2%), and muscovite (<1%) (Catt et al., 1975). In contrast to the Helsby Sandstone formation, the sandstone at Woburn is nearly matrix-free and uncemented, and the interstices exhibit negligible (0.1%) clay content (Catt et al., 1975; Palmer and Barton, 1987). The porosity has been previously reported as 35% with little evidence found of porosity reduction based on the small proportion of ductile clasts and the moderate sorting (Palmer and Barton, 1987). A detailed mineralogical analysis of the Lower Greensand Group at Woburn is provided by Catt et al. (1975) and further assessments of the parent material at nearby sites can be found in Rastall (1919). Extensive analysis suggests that the provenance of the Lower Greensand at Woburn is marine-based (Stead and Eyers, 2017). Although there is much dispute in the literature about the mechanisms of its formation, many scholars believe that the Woburn sandstone developed from an offshore tidal sand wave deposit in shallow water conditions (Stride, 1982; Eyers, 1991; Owen, 1992). This marine-based sandstone cut into the Late Jurassic mudstones between the late Aptian and early Albian (126–100 Ma) during the Cretaceous period (Catt et al., 1975).

Both sites are positioned within the Anglian glaciation (~450,000 BP). Although both sites are located beyond the areal extent of the Late Devensian ice sheet (~20,000 BP) (Eyles et al., 1994; Gibbard and Clark, 2011), evidence suggests that periglacial conditions are likely to have dominated at these latitudes during this period (Watson and Morgan, 1977; Tye et al., 2012). Hilton is positioned beyond the areal extent of the British-Irish ice sheet at the Last Glacial Maximum (LGM; ~21,000 BP) (Gibbard and Clark, 2011). However, there is some debate as to whether this area was covered, if only partly, during the earlier stages of the Devensian glaciation (Bowen et al., 2002; Evans et al., 2005). The site sits within the 'Wolverhampton Line' (Shotton, 1967) which represents the terminal position of the Irish Sea Glaciation and nearby the site are a number of drift and till deposits (Hollis and Reed, 1981). The area is likely to have been dominated by broadleaf woodland between 6000 and 2000 BCE, and heathland until the late 19th century. By 1883, Hilton was under agriculture, and this was most likely to have been pastoral (Fullen, 2020).

At Woburn, the study site and surrounding area was blanketed in boulder clay after the retreat of the Anglian glaciation. This was subsequently eroded, leaving a thin decalcified remnant of this clay incorporated into the Lower Greensand through processes of cryoturbation

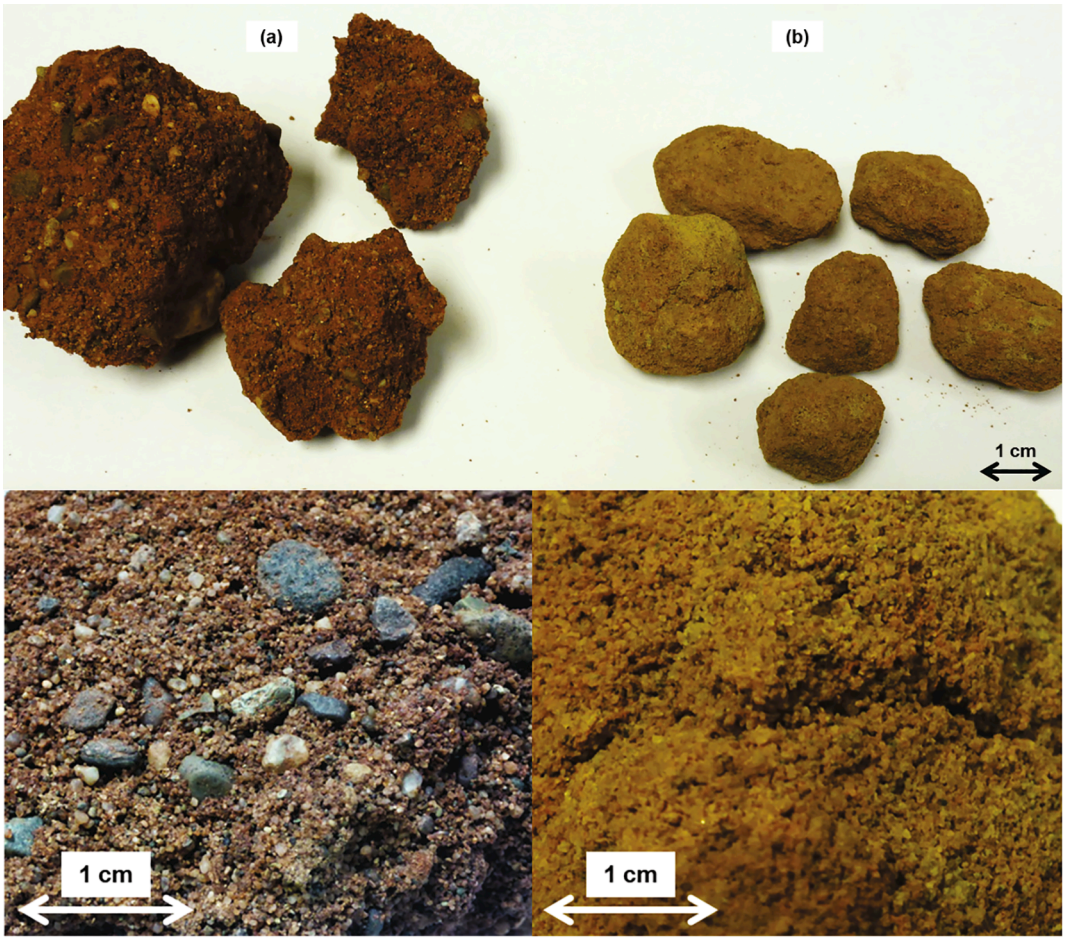

Fig. 2. Photographs of the saprolite at (a) Hilton and (b) Woburn.

(Catt et al., 1975). Particle size analysis conducted by the authors suggests that this boulder clay has not been incorporated into the soils at the study site; a finding similarly observed by Catt et al. (1975). The site would have been dominated by periglacial conditions during the Late Devensian (Gibbard and Clark, 2011). Catt et al. (1975) suggests that forests were cleared in the Middle to Late Bronze Age (~3000 years ago), when the soils were first cultivated.

2.2. Sampling and processing soil and saprolite

2.2.1. Sampling saprolite

Summit, shoulder, backslope and toeslope positions on both catenas were selected for depth to bedrock surveys, as well as soil and saprolite extraction. At each position, a dynamic cone penetrometer was employed to ascertain the approximate depth of the soil-saprolite interface before a soil pit was dug vertically to this zone. Variations in the consolidation of the profile wall were observed by extracting small cores down the profile and noting the extent to which the material remained intact. These observations were then compared with the penetration resistance data to confirm the depth of the soil-saprolite interface. Samples of saprolite of between 5 and 10 cm thickness were extracted from each interface for cosmogenic radionuclide analysis. A further sample was then extracted approximately 30 cm below this interface.

2.2.2. Cosmogenic radionuclide analysis

Beryllium-10 is produced when quartz grains within the uppermost metres of bedrock are bombarded with cosmic rays. If the intensity of these cosmic rays and the weathering of the bedrock (ε) is assumed to be constant, the concentration of ^{10}Be (N) in a sample of bedrock is dependent upon the time that the bedrock has been exposed to cosmic rays, and the rate at which bedrock weathers into mobile regolith (soil). Short exposure times and fast rates of bedrock weathering both lead to lower concentrations of ^{10}Be, and vice versa (Lal, 1991; Stockmann et al., 2014). We assume here that ^{10}Be production and bedrock denudation is at equilibrium.

$$N = \sum_{i=sp,\mu_f,\mu^-} \frac{P_i(\theta) \bullet e^{-\frac{x}{\Lambda_i}}}{\lambda + \frac{\epsilon\rho}{\Lambda_i}} \left(1 - e^{-t\left(\lambda + \frac{\epsilon\rho}{\Lambda_i}\right)}\right) \quad (1)$$

where: N is the concentration of ^{10}Be (atoms/g), P are the annual production rates of ^{10}Be by spallation, fast muons and stopping muons (atoms/g/year) (denoted by subscripts sp, μf and μ-) at a surface with slope Θ; x is the mass sample depth ($\rho \bullet z$) (cm); p is the density of overburden material (g/cm^3); z is the depth of the sample (cm); t is the age of the bedrock surface (the age when the original surface was generated) (years); λ is the decay constant of ^{10}Be with λ equalling In2/^{10}Be half-life; and Λ are the mean attenuation thicknesses of cosmic radiation for different production pathways (cm) (Lal, 1991). Here, we considered t as infinite to calculate the apparent weathering rate ε, assuming that the age of the landscape is old enough for the ^{10}Be depth-profile to be in equilibrium. By studying two samples down the same depth profile, we tested whether the data met this assumption. By measuring N using Accelerator Mass Spectrometry (AMS), Eq. (1) was solved for ε by simple interpolation of N.

A total of sixteen samples of saprolite (eight from Hilton and eight from Woburn) were prepared for AMS at the Cosmogenic Isotope

Analysis Facility, East Kilbride, Scotland. After mineral separation, quartz cleaning, and procedures leading to the preparation of BeO sample cathodes (Kohl and Nishiizumi, 1992; Fifield, 1999; Corbett et al., 2016), AMS measurements were carried out at the SUERC AMS laboratory (Xu et al., 2010). ^{10}Be concentrations were based on 2.79 x10^{-11} ^{10}Be/^{9}Be ratio for the NIST Standard Reference Material 4325. The processed blank ratio ranged between 5 and 24% of the sample ^{10}Be/^{9}Be ratios. The uncertainty of this correction is included in the stated standard uncertainties.

As first demonstrated in Evans et al. (2020b), the interpolation of N to solve for ε must account for the variability in the density of the soil above the point of sampling because the overburden density exerts an influence on the attenuation of cosmic rays down the profile. The CoSOILcal model (Rodés and Evans, 2019) calculates a best-fit bedrock lowering rate accounting for either estimated or, preferably, empirically measured bulk density data of the soil profile overlying the bedrock surface. This model was applied in this study to calculate soil formation rates using empirically measured soil bulk densities from each catena position, at both sites. In addition, the annual production rate of ^{10}Be was calculated, accounting for obstructions that would reduce the cosmic ray flux to the parent material (Phillips et al., 2016; Evans et al., 2019). These local ^{10}Be production rates were normalized by inputting site elevation, latitude and longitude data into the CRONUS-Earth Matlab code v2.3 using Lal/Stone (St) scaling (Balco et al., 2008). Version 2.3 incorporates the reference production rates derived from Borchers et al. (2016).

Whilst Eq. (1) can be used to derive soil formation rates in absolute terms, soil formation rates are partly governed by soil thickness. A key objective in this study is to investigate the effect of lithology on soil formation rates, rather than soil thickness. Therefore, it is necessary to calculate soil formation rates across the sites for a given soil thickness. It is commonplace in these cases to calculate for zero soil thickness, and this is achieved by deriving the soil production function (P):

$$P = We\left(\frac{-h}{\gamma}\right) \tag{2}$$

where W is the soil formation rate at zero soil thickness (h) and γ determines the soil thickness when soil formation is reduced by $1/e$ (Dietrich et al., 1995; Heimsath et al., 1997). Both W and γ, and their respective uncertainties, were calculated from measured rates of soil formation and corresponding soil thicknesses using a Monte-Carlo simulation run in Matlab ($n = 1000$; see Supplementary Information).

2.2.3. Scanning electron microscopy

Freshly exposed surfaces of saprolite extracted from the soil-saprolite interface at both sites were prepared for scanning electron microscopy (SEM). Samples were affixed to aluminium SEM stubs (12 mm diameter) using Leit-C conducting carbon cement, and coated to a thickness of 25 nm using a carbon coater. The analysis was carried out at the British Geological Survey's scanning electron microscopy laboratory using a Zeiss Sigma 300 field emission SEM. In order to analyse the topography and surface structure of the samples, an ET-SE detector was used to detect secondary (SE2) electrons. An In-lens detector was subsequently deployed to analyse the surface structure at greater magnification. The acceleration voltage (U_{EHT}) was 10 kV, the aperture was 30 μm, and images were captured at a 1024×768 resolution using scan speed 10.

2.2.4. Analysis of soil samples

Soil samples were extracted every 10 cm from the profile wall of each catena position at both sites. These samples were then oven dried at 105 °C for twelve hours, grounded with a pestle and mortar, and sieved to remove the > 2 mm fraction. Using these samples, stone-corrected bulk density measurements were calculated. A Beckman Coulter Laser Diffraction Particle Sizing Analyser LS 13 320 was employed for particle size analysis (pump speed: 70%; sonication: 10 s; run length: 60 s). LOI content was determined from separate 5 g sub-samples using mass loss following heating at 550 °C for twelve hours in a Carbolite furnace (CWF 1300).

3. Results

3.1. Soil analysis

At Hilton, the soils are classified as Arenosols (IUSS Working Group WRB, 2014) and are of a coarse sand texture, with the mean particle size distribution being 80% sand, 15% silt, and 5% clay (Fullen, 1991). At the summit, the A horizon is 30 cm in thickness with a mean bulk density of 1.4 g/cm^3, below which lies a 75 cm B horizon with a mean bulk density of 1.6 g/cm^3. The soil-saprolite interface is observed at 105 cm, below which the profile grades into saprolitic, moderately consolidated sandstone. The LOI content decreases from 5.0% in the A horizon to 0.9% in the underlying subsoil. At the shoulder, the A horizon is 10 cm thick and, in places, it is less distinct. The loose and friable nature of the soil at the surface explains its relatively low bulk density: 1 g/cm^3. The B horizon extends to 80 cm, below which the material becomes more consolidated (mean bulk density is 1.4 g/cm^3) and saprolitic. Here, the A horizon has a LOI content of 4.9%. This contrasts with the B horizon where the mean LOI content is 1.0%. The thinnest soil is found at the backslope, with the soil-saprolite interface observed at 50 cm. The soil comprises a 10 cm A horizon, and like the shoulder, has a relatively low bulk density of 0.8 g/cm^3. The B horizon is 40 cm and has a mean bulk density of 1.3 g/cm^3. The LOI content of the A horizon is 4.2%. Below this, the mean LOI content falls to 2.2%. Finally, the soil at the toeslope is 100 cm thick. Although this is also the case for the summit, the toeslope profile exhibits a comparatively thicker A horizon (40 cm) suggesting that colluviation has, or is still, happening at this position. However, the presence of a grass and shrub cover at Hilton suggests that colluviation rates are currently slow, if not negligible. Despite the thicker A horizon, the mean LOI content (3.1%) is smaller than that observed for the summit, but the mean bulk density is similar (1.4 g/cm^3). In the 60 cm B horizon, the mean LOI content falls to 1.5% and the mean bulk density is 1.5 g/cm^3.

At Woburn, the soils are also classified as Arenosols (IUSS Working Group WRB, 2014). Both the topsoil and subsoil at each hillslope position have a coarse sand texture, with the mean particle size distribution being 83% sand, 10% silt, and 7% clay (Quinton and Catt, 2004). At the summit, an Ap horizon of 30 cm thickness, with a mean bulk density of 1.2 g/cm^3, overlies an iron pan between 30 and 70 cm. This was a hardpan horizon, principally cemented by iron oxides, which did not disaggregate when subject to manual pressure in the field. The consequential greater density of this iron pan (1.6 g/cm^3), and the effect on the attenuation of cosmic rays, is accounted for. The CoSOILcal model, employed in this study to calculate soil formation rates from measured ^{10}Be concentrations, considers the density profile of the soil overlying the soil-saprolite interface (Rodés and Evans, 2019). At the bottom of this iron pan is the soil-saprolite interface, under which lies moderately consolidated, cross-bedded saprolitic sandstone with a mean bulk density of 1.5 g/cm^3. The LOI content decreases from 2.5% in the Ap horizon to 1.5% in the underlying subsoil to a depth of 100 cm. The iron pan observed at the summit is not present down the soil profiles at the other hillslope positions surveyed. At the shoulder and backslope, the thickness and mean bulk density of the Ap horizon is 27 cm (1.4 g/cm^3) and 30 cm (1.5 g/cm^3), respectively, and both are underlain by an undifferentiated subsoil, extending down to 40 cm at the shoulder (incidentally, the shallowest soil down the catena) and 66 cm at the backslope. The mean bulk density for both the shoulder and backslope B horizons is 1.5 g/cm^3. The LOI content at the shoulder and backslope also demonstrates similar trends to the summit, with the Ap horizon having a LOI content between 2.1 and 2.2% which decreases to 0.8–1.0% in the B horizon. At the toeslope, there are two distinct A_1 and A_2 horizons; an A_1 mantle extending from the surface down to 35 cm

(with a mean bulk density of 1.3 g/cm^3) burying an A_2 horizon that extends down to 50 cm (with a mean bulk density of 1.6 g/cm^3). The B horizon is similar to that observed at the shoulder and summit, with a density of 1.5 g/cm^3, except for the fact that this horizon extends to 170 cm, making this profile the thickest. The toeslope also has the greatest LOI content, with 2.9% in the A_1 horizon, 2.1% in the A_2 horizon, and 1.2% in the B horizon. The presence of an A_p horizon at each catena position may be explained in part by the mixing of mineral and organic material through cultivation following the harvest, although isotopic work at Woburn is required to verify this.

3.2. Soil formation rates

Soil formation rates were calculated from measured ^{10}Be concentrations at Hilton and Woburn (Table 2; Fig. 3). At Hilton, soil formation rates range from 0.065 to 0.193 mm yr^{-1}, while at Woburn these range from 0.031 to 0.150 mm yr^{-1}.

4. Discussion

4.1. Soil formation rates in the UK context

Fig. 4 compares these rates with those previously calculated for two other sandstone sites in the UK: Rufford Forest Farm, in Nottinghamshire, and Comer Woodland, in Shropshire (Evans et al., 2019). Like Hilton, the soil at Rufford Forest Farm (Rufford, hereafter) has formed from the Sherwood Sandstone (Chester formation, Olenekian, 247–251 Ma) which has been described as fluvially-derived, pinkish to red, medium to coarse grained, pebbly, cross-bedded and friable (see Radley and Coram, 2016). In contrast, the soils at Comer Wood (Comer, hereafter) stem from the New Red Sandstone (Bridgnorth formation, Cisuralian, 273–299 Ma). This sandstone is of aeolian origin, and has been described as brick-red, medium grained, and cross-bedded (British Geological Survey, 2020). Further contextual details about Rufford and Comer can be found in Evans et al. (2019).

Data from these sites suggest that soil formation rates are slower under thicker soil profiles (such as those observed at the summit and toeslope positions). This largely supports the conclusions previously observed for two other sites in the UK (Evans et al., 2019). Under a thicker soil, the bedrock is buffered more effectively from climate fluctuations, organism activity at the surface, and other subaerial factors that may promote soil formation (Minasny and McBratney, 1999; Wilkinson and Humphreys, 2005).

The soil production function (Eq. (2)) was used to estimate the depth over which soil formation decays by 1/*e*. This depth is referred to as the 'Gamma value' (see Eq. (2); Table 3) and indicates the sensitivity of soil formation rates to soil thickness. This ranges from 0.80 ± 0.10 m at Woburn to 4.50 ± 1.80 m at Comer, demonstrating at least 1.8 m variation in the sensitivity of soil formation to soil thickness between these sites. Given that soil thickness, and the sensitivity of soil formation to soil thickness, differs between sites, we will focus our analysis hereafter on the rates of soil formation calculated for zero soil thickness, using the soil production function (Eq. (2)). Based on a Monte Carlo simulation (see Supplementary Information), Table 3 shows that soil formation rates for Woburn are greater than the upper bounds of uncertainty of the three other sites. Furthermore, soil formation at Hilton is approximately 1.5x slower than that at Woburn, but more than double the rates observed at both Comer and Rufford.

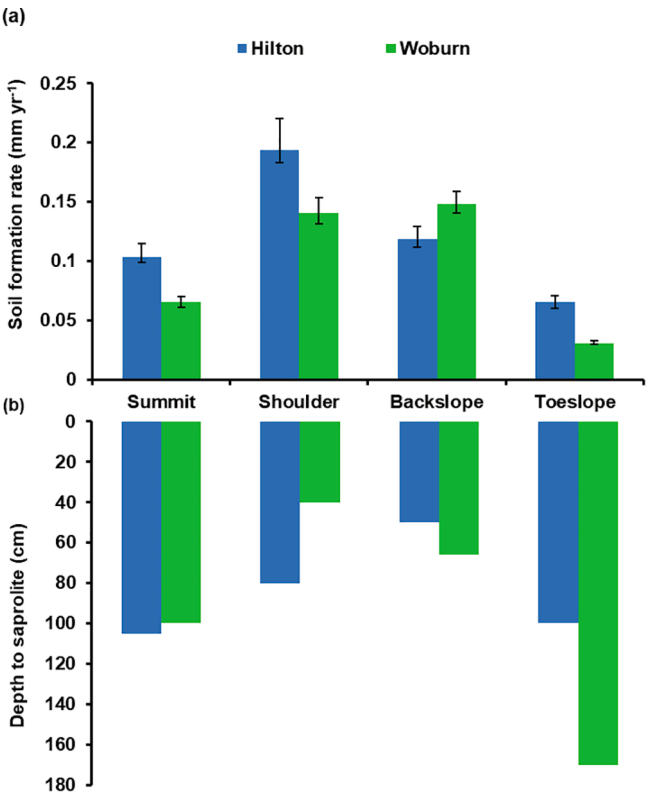

Fig. 3. Soil formation rates and depths to saprolite for the four sampling positions along the catena transects at Hilton (blue; $n = 4$) and Woburn (green; $n = 4$). Error bars on soil formation rates indicate 1σ uncertainties. Two ^{10}Be concentrations down the same depth profile have been used in the CoSOILcal model to derive a "best fit" soil formation rate (see *Methods*).

Table 2
^{10}Be concentrations and calculated soil formation rates for Hilton and Woburn.

Site	Catena Position	Sampling Depth (mm)	Latitude	Longitude	Shielding correction	10Be concentration (atoms g-1)	Uncertainty in 10Be concentration (atoms g-1)	Soil Formation Rate (mm yr)
Woburn	Summit	1000	52.01265	−0.590347	0.999993	38,324	2081	0.0653483
Woburn	Summit	1500	52.01265	−0.590347	0.999993	Failed	Failed	Failed
Woburn	Shoulder	400	52.01249	−0.590342	0.999882	27,931	2215	0.1407499
Woburn	Shoulder	900	52.01249	−0.590342	0.999882	18,129	1710	0.1495048
Woburn	Backslope	660	52.01224	−0.590299	0.999952	21,863	1553	0.1485079
Woburn	Backslope	1060	52.01224	−0.590299	0.999952	20,488	1695	0.117606
Woburn	Toeslope	1700	52.01182	−0.590253	1	49,291	2592	0.030903
Woburn	Toeslope	2200	52.01182	−0.590253	1	27,384	4009	0.0450818
Hilton	Summit	1050	52.55159	−2.323442	0.999753	26,958	1933	0.1033382
Hilton	Summit	1400	52.55159	−2.323442	0.999753	24,110	2637	0.1534478
Hilton	Shoulder	800	52.55156	−2.323781	0.998285	15,983	1525	0.1933713
Hilton	Shoulder	1100	52.55156	−2.323781	0.998285	15,878	1541	0.1631211
Hilton	Backslope	500	52.55152	−2.324105	0.998391	32,121	2373	0.1186757
Hilton	Backslope	700	52.55152	−2.324105	0.998391	22,656	1797	0.1436933
Hilton	Toeslope	1000	52.55147	−2.324557	0.999995	35,605	5203	0.0651254
Hilton	Toeslope	1300	52.55147	−2.324557	0.999995	22,512	1564	0.0866683

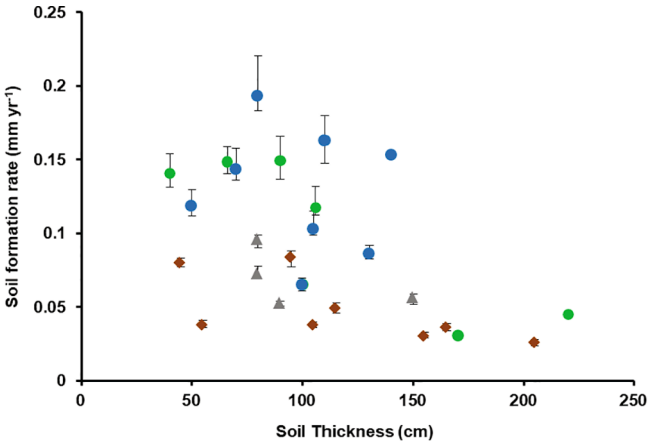

Fig. 4. Soil formation rates against soil thickness for Hilton (blue; $n = 8$) and Woburn (green; $n = 7$) with those previously measured by Evans et al. (2019) at Rufford Forest Farm (brown diamonds; $n = 8$) and Comer Wood (grey triangles; $n = 4$). The error bars represent one standard deviation uncertainties.

4.2. Lithological variability – The role of sandstone matrices

4.2.1. Soluble fraction

Given that the data here stemmed from one climate, we suggest that the variation in soil formation can be explained by the different diagenetic conditions that formed contrasting sandstone lithologies. At both Hilton and Woburn, during initial sandstone formation, the dominant environmental conditions suggest that evaporitic minerals and soluble cements may have composed part of the matrix material. In the case of the Helsby sandstone formation at Hilton, the climatic conditions of the Triassic period would have led to the extensive formation of evaporite minerals within the rock. In *confined* Sherwood Sandstone aquifers, to which meteoric waters have not gained access, evaporite minerals are still observable today (Burley, 1984). However, for unconfined aquifers, such as the Helsby sandstone at Hilton, isotope evidence suggests that these Triassic evaporites subsequently dissolved as a result of being flushed with cool, fresh, meteoric waters (Burley, 1984), potentially during the Pleistocene (Downing et al., 1987; Tellam, 1995). Similarly, the marine provenance of the sandstone at Woburn suggests that calcite would have been abundant in the initial depositional stages, but this would have also dissolved rapidly. This is evidenced by Tye et al. (2012) whose work on the Sherwood Sandstone formation showed that CaO concentrations are negligible (<0.5%) in the upper 17 m of the sequence. This work, along with the absence of soluble minerals in this study's SEM analysis, suggests that the soluble fraction of the sandstone matrix does not influence rates of soil formation since it has already been weathered out of the soil–saprolite interface.

4.2.2. Depth of burial

We suggest the predominant factor influencing the strength of the sandstone and its resistance to weathering is the depth of burial, and the diagenetic processes associated with the corresponding burial temperatures and pressures. The consequence of a deeper burial in the Sherwood Sandstone group would have been to increase grain-to-grain contacts within the bedrock. This ratio expresses the difference between the length of contact a grain has with its neighbouring grains, and its own individual length (Dyke and Dobereiner, 1991). Previous work elsewhere has demonstrated a strong relationship between grain contact and the strength of sandstone (Dobereiner, 1984). SEM analysis of the saprolite at Hilton shows evidence of compaction-induced dissolution on grain contact sites. For example, Fig. 6d shows topographic depressions on the roughened grain surfaces which are most likely the products of increased grain-to-grain contacts. Elsewhere, euhedral microcrystals of quartz have formed at the grain contact sites revealing evidence of contact dissolution and reprecipitation processes. The presence of quartz microcrystals between the grains of the Helsby sandstone at Hilton would serve to strengthen the integrity of the sandstone, further reducing its susceptibility to weathering.

Bloch et al. (2002) found that greater temperatures (>100 °C) associated with deeper burials can lead to quartz dissolution, which subsequently results in the precipitation of quartz cements. These quartz cements can bind as overgrowths to the uncoated surfaces of mineral grains within the sandstone, and strengthen their physical integrity. In accordance with this, SEM analysis of the sandstone at Hilton reveals evidence of quartz overgrowths that have formed as minor yet widespread diagenetic cements that occlude the porosity between grains (Fig. 6d). The additional strength provided by these overgrowths would further reduce the susceptibility of the sandstone to weathering processes. Furthermore, an increase in the grain-to-grain contact ratio in the Sherwood Sandstones would have reduced the intergranular pore volumes. A consequence of this is that a relatively smaller volume of cementing agents would have been required to cause cohesion between these mineral grains. In Hilton, Comer, and Rufford, iron oxides (mostly in the form of hematite) have often been shown to cause this intergranular welding. The formation of hematite predominantly occurred as a result of the alkaline Triassic groundwaters oxidising iron into ferric oxide. The red pigmenting exhibited in Fig. 2a demonstrates the presence of hematite in the saprolite underlying Hilton. Moreover, SEM analysis of this sandstone also revealed evidence of well-developed K-feldspar overgrowths (Fig. 6b) cementing grains together.

By contrast, the shallow burial of the sandstone at Woburn would have resulted in a different array of diagenetic conditions. The relatively lower temperatures and pressures would have reduced quartz dissolution reactions and the subsequent precipitation of quartz overgrowths. This study's SEM analysis did not reveal evidence of quartz overgrowths in the Woburn sandstone. This supports previous work by Palmer and Barton (1987) who found a relative absence of quartz overgrowths in this sandstone when compared with similar lithologies, such as the Wyoming Sands. Moreover, the lack of iron oxides in the sandstone at Woburn may be a legacy of the marine conditions in which the sandstone was laid. Seawater has a relatively low concentration of iron (Bloch et al., 2002) which may explain why the saprolite exhibits less evidence of hematite. In addition, SEM analysis did not show evidence of any other intergranular cement or K-feldspar overgrowth. On the contrary, some areas revealed clean quartz grain surfaces (Fig. 5b). The absence of quartz overgrowths, iron oxides, and K-feldspar may explain why the Woburn sandstone is less cemented and, instead, more susceptible to weathering.

Table 3
Soil formation rates for each of the four sites in this paper.

		Comer	Hilton	Rufford	Woburn
Sandstone formation		Bridgnorth	Helsby	Chester	Woburn
Gamma value (m)[a]		4.50 ± 1.80	2.70 ± 1.20	2.27 ± 0.38	0.80 ± 0.10
Soil Formation Rate (mm y^{-1})	*Range*	0.053–0.096	0.065–0.193	0.026–0.084	0.031–0.150
	Zero soil thickness[b]	0.077 ± 0.009	0.175 ± 0.039	0.071 ± 0.006	0.274 ± 0.045

[a] Calculated soil thickness when soil formation is reduced by $1/e$ using the soil production function (see Eq. (2) in *Methods*).
[b] Soil formation rates (and one sigma uncertainties) calculated using the soil production function (see Eq. (2) in *Methods*).

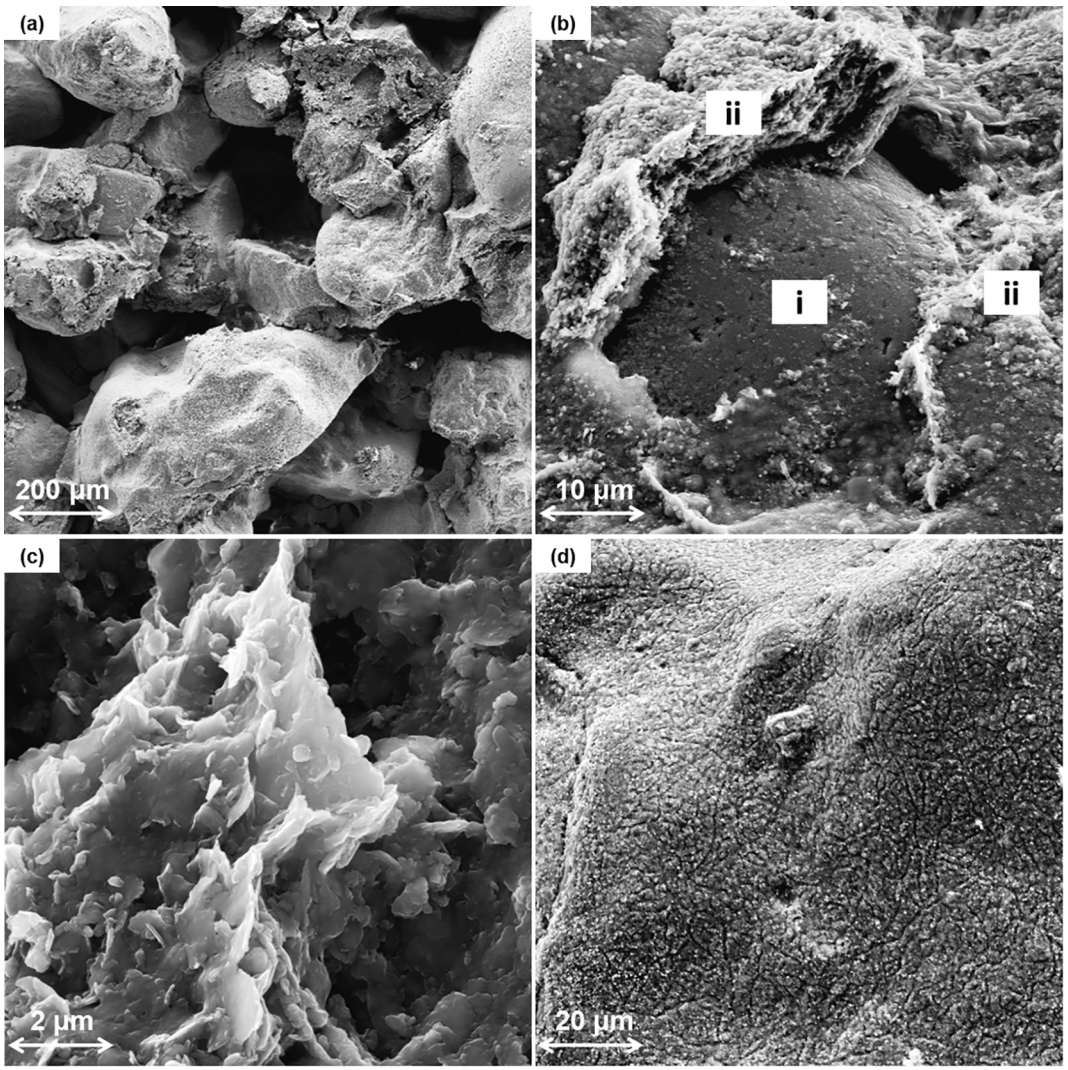

Fig. 5. SEM images of saprolite extracted from the soil-saprolite interface at Woburn; (a) General view showing moderately poor sorting with very fine to coarse grains, with infiltrated clay thickly distributed throughout; (b) Clean quartz grain contact site (*i*) with hardly any clay coating and no evidence of contact dissolution, surrounded by typical infiltrated clay ridges (*ii*); (c) Detail of infiltrated clays showing highly variable particle size, and platy clays with roughened edges; (d) Desiccation texture exhibited in well-developed infiltrated clay bridging between grains.

4.2.3. Clays

Another example of a matrix mineral previously shown to give structural integrity to saprolite is clay. Heimsath and Whipple (2019) present a conceptual model that builds on earlier work which suggests that as soils develop and thicken from the underlying saprolite, soil formation rates decrease. This induces a delay in the formation of soil from saprolite (Heimsath and Whipple, 2019) and consequently leads to some clays and secondary minerals forming within it that may act to retain some structural integrity for longer. In a similar way that soil shear strength increases with greater clay content (Stark and Eid, 1994), Heimsath and Whipple (2019) suggest that the clays which begin to accumulate within the saprolite can increase its resistance to further physical weathering or disruption by helping to retain its structural integrity, thus reducing rates of soil formation. Although the authors do not present measured clay contents, they do show that the shear strength of saprolite increases as the overlying soil thickens, and propose that original clay or re-precipitated clay formation plays a large role in maintaining some structural integrity within the saprolite. In addition, percolation theory also suggests that the accumulation of clays would decrease chemical weathering reactions by reducing rates of the infiltration and transport of water through the saprolite (Hunt and Ghanbarian, 2016).

SEM analysis conducted here shows that the spatial distribution of clay within the sandstone differs between Hilton and Woburn. At Woburn, the clays are pore-lining, rather than pore-filling, suggesting a negligible ability to reduce sandstone porosity. Detailed imaging demonstrates that the edges of these clays are rough and angular (Fig. 5c). The absence of smooth and/or euhedral forms to the clay edges indicates that these clays are not of diagenetic origin, and are instead allogenic. In other words, the clay was emplaced into the sandstone via infiltration, most likely during soil formation processes that occurred much later (Matlack et al., 1989). Where clay particles are orientated perpendicular to the quartz grains, these form distinct ridges around grain contact sites (Fig. 5b). Where clay particles are aligned in parallel with the quartz grains, the clay occurs as granular sheet-like grain coatings (Fig. 5d). Interestingly, these grain coatings exhibit a desiccation-like texture which we speculate could be evidence of multiple episodes of shrinking and swelling. Although further chemical analysis of the clays is required, this process may help to break the physical bonds between the grains in the Woburn sandstone, thus further reducing its structural integrity, and increasing its susceptibility to weathering.

At Hilton, SEM analysis reveals evidence of infiltrated clay ridges and grain coating clays, with many clay ridges having formed on top of other diagenetic features like K-feldspar overgrowths. Unlike the sandstone at

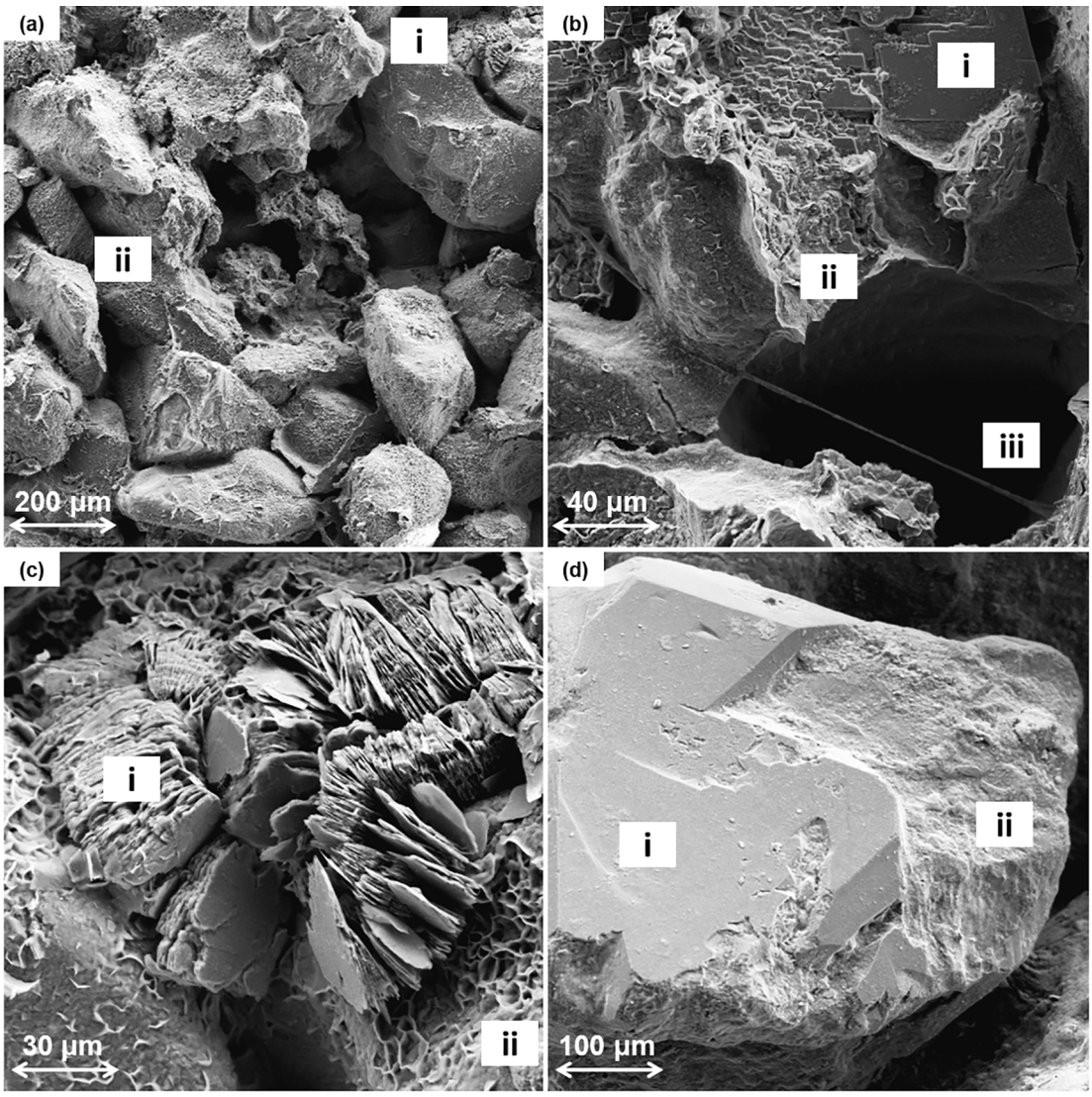

Fig. 6. SEM images of saprolite extracted from the soil-saprolite interface at Hilton; (a) General view showing a fine to medium grained, moderately well-sorted sample, with kaolinite books (*i*) and K-feldspar (*ii*) cements; (b) Well-developed K-feldspar overgrowth (*i*) partially covered by infiltrated clays that have subsumed kaolinite (*ii*) pore-bridging (probably fungal) filament (*iii*); (c) Interlocking cluster of coarse (>30 μm) pore-filling kaolinite (*i*) and webbed box work diagenetic grain-coating illite clays (*ii*); (d) Thin but well-developed quartz overgrowth (*i*) with some exposed grain contact sites (*ii*) showing slight surface depressions indicating compaction dissolution.

Woburn, interlocking clusters of coarse (>30 μm) diagenetic, pore-filling kaolinite are particularly abundant at Hilton (Fig. 6b and c), which has been reported previously (Huggett, 1982). The presence of these pore-filling clays has the effect of partially blocking pore throats, thereby diminishing the infiltration and storage of meteoric waters and decreasing weathering susceptibility.

4.2.4. Comparison with global inventory

Fig. 7 compares soil formation rates from Hilton and Woburn with those from other sandstone-derived soils taken from the published literature (n = 48; Supplementary Information). Scholars have previously shown that climate is one of the most influential factors in constraining rates of soil formation (Stockmann et al., 2014). Therefore, in order to reduce the influence that climate may have on this analysis, the data that comprise this global inventory stem from temperate climates only.

The data from the global inventory demonstrate a slight reduction in soil formation rates as soils thicken. In accordance with previously published analyses, soil formation rates fall by more than an order of magnitude between soil thicknesses of 0 and 50 cm. Between 50 and 100 cm, this decline is less pronounced with rates oscillating between ~ 0.01 and 0.06 mm yr^{-1}. Comparing the data from both this study and Evans et al. (2019), with those from the published inventory, presents two important findings.

First, for soils between 40 and 100 cm deep, soil formation rates from Hilton and Woburn are similar to those from the global inventory. The pattern is one of quasi steady-state where rates do not significantly decline with increasing soil thickness and, instead, are enveloped within a range (~0.07–0.19 mm yr^{-1}). However, in the majority of instances, the rates from Hilton and Woburn are towards the upper end of, if not greater than, those previously published.

Second, for soils deeper than 100 cm, the data from Hilton and Woburn shows a linear negative relationship between soil formation rates and soil thickness. Given that there is only one rate presented for soils deeper than 100 cm from the global inventory, the data from Hilton and Woburn, together with those from Comer and Rufford, represent an important contribution to our knowledge of soil formation for deeper soils.

One explanation for why soil formation rates at Hilton and Woburn are towards the upper end of, if not greater than, those previously

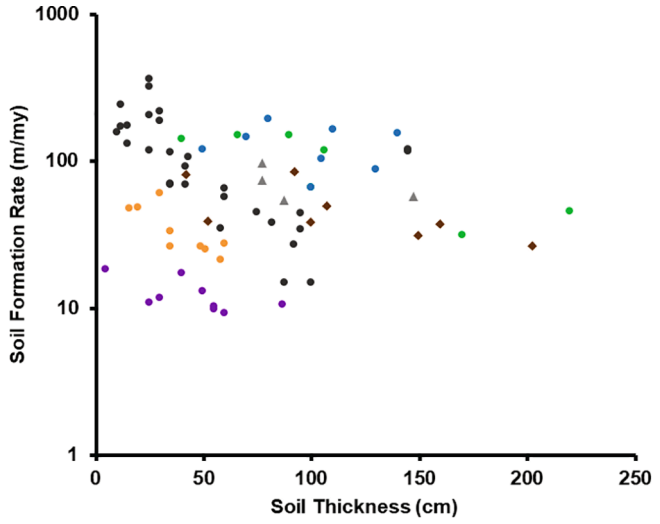

Fig. 7. Soil formation rates from Hilton (blue; $n = 8$) and Woburn (green; $n = 7$), together with those from Rufford Forest Farm (brown diamonds; $n = 8$), Comer Wood (grey triangles; $n = 4$) and those from a globally compiled inventory of soil formation rates on sandstone geology from Heimsath et al., 1997 (orange circles; $n = 9$), Heimsath et al., 2001 (grey circles; $n = 30$), and Wilkinson et al., 2005 (purple circles; $n = 9$).

published could be because of the volume and composition of the sandstone matrices. Many of the sandstones previously studied are classified as 'wackes' (using the Pettijohn et al., 1987 scheme) due to the fact that 15% of their rock volume is matrix material. This contrasts with the arenite sandstones found at Hilton and Woburn, where the matrix material comprises <15% of the total rock volume. Here, there is less cohesion between the framework grains of the bedrock, implying a relatively weaker structural integrity, and a greater susceptibility to weathering processes.

For example, Wilkinson et al. (2005) conducted work on the Blue Mountains in Australia, where the parent material was a moderately to strongly lithified Triassic sandstone, dominated by cobbles of ferruginous sandstone that are resistant to weathering. These were neither observed at Woburn nor at Hilton. At 50 cm, the soil formation rate on the Blue Mountains was nine times slower than that at Hilton for the same soil thickness. We believe that the bands of relatively resistant sandstone, cemented by an iron-enriched matrix, are in part responsible for the slower soil formation rates measured on the Blue Mountains. Similarly, Heimsath et al. (2001) measured soil formation at Coos Bay, located along the Oregon coast range, in the USA. The soils are underlain by an Eocene arkosic wacke: a sandstone with a matrix comprising >15% by volume, and >25% feldspar. At 100 cm, the soil formation rate at Coos Bay was 0.014 mm yr^{-1}, five times slower than that at Woburn, where the absence of this matrix promotes the transmission of water and weathering processes (Cummins, 1962).

5. Conclusions

In this study, we have investigated the extent to which the lithological variability of sandstone governs rates of soil formation. Cosmogenically-derived rates of soil formation for two UK hillslopes range from 0.031 to 0.193 mm yr^{-1}, with rates at zero soil thickness being 0.175 ± 0.039 mm yr^{-1} and 0.274 ± 0.045 mm yr^{-1} at Hilton and Woburn, respectively. In addition to being only the second study in the UK to measure soil formation for soils currently supporting arable agriculture, the sandstone-derived soils studied here represent some of the deepest profiles that have been subject to cosmogenic radionuclide analysis.

We found that the soil formation rates measured at Woburn are faster than those measured at Hilton, and we suggest here that this may be substantially governed by the lithological variabilities exhibited between the two sandstone formations. The temperatures and pressures associated with a deeper burial at Hilton would have led to the cohesion of mineral grains by intergranular cements, such as quartz and K-feldspar overgrowths. As well as holding the framework grains together, another effect of these cementing agents is to slow down the transmission of water through the bedrock and reduce rates of chemical weathering. SEM evidence suggests that this cementation is less abundant at Woburn, which could explain why soil formation rates are faster at this site.

Although there is disparity between the Helsby and Woburn sandstone formations, both of these lithologies contrast with those that have been previously investigated in studies of soil formation. The rates from the sandstones of Hilton and Woburn are, in some cases, up to nine times faster than those procured previously by researchers working on wackes. Here, we suggest that the matrix-abundant wackes reduce the transmission of water and slow the process of soil formation. These findings highlight the need for a greater insight into the mineralogy and petrology of the parent material when interpreting rates of soil formation.

Our work has opened a new gap for soil formation research. This community has hitherto measured soil formation rates and compared them across major rock types (igneous, sedimentary, and metamorphic). Our study suggests that the role of the mineralogical and petrographic variations within a single rock group in governing rates of soil formation warrants further exploration. Having shown here the breadth of soil formation rates for different types of sandstone, more work is required to study other sedimentary units and different types of igneous and metamorphic rock.

6. Financial support

This work was partly supported by BBSRC and NERC through a Soils Training and Research Studentships (STARS) grant (no. NE/M009106/1) and partly by a NERC research grant (no. CIAF 9191/1018). STARS is a consortium consisting of Bangor University, the British Geological Survey, the Centre for Ecology and Hydrology, Cranfield University, the James Hutton Institute, Lancaster University, Rothamsted Research and the University of Nottingham.

7. Data availability

All related data can be found in the Supplementary Information.

Author contributions

DLE, JNQ, AMT and JACD designed the research. DLE, JNQ and AMT conducted sampling. AR and DLE conducted cosmogenic laboratory work and analysed results. JR, AT and DLE conducted SEM analysis. DLE prepared the paper with contributions from all co-authors.

Declaration of Competing Interest

The authors declare that they have no known competing financial interests or personal relationships that could have appeared to influence the work reported in this paper.

Acknowledgements

The authors wish to thank Steve McGrath, Stephen Goward, Andy Macdonald, Ian Shield and Robert Copley for permission to carry out fieldwork at Woburn Experimental Farm, and Mike Fullen, Andrew Black and Richard Wills for permission to sample at Hilton Experimental Site. We thank Phil Styles and Robert Tuckwell for fieldwork assistance at Woburn, and likewise, Pedro Velloso Gomes Batista and Miroslav Bauer for their support at Hilton. We also wish to thank Allan Davidson,

Ángel Rodés, Derek Fabel at the NERC Cosmogenic Isotope Analysis Facility for preparing samples for AMS and their subsequent assistance in data analysis. We thank three anonymous reviewers for providing constructive feedback.

Appendix A. Supplementary data

Supplementary data to this article can be found online at https://doi.org/10.1016/j.geoderma.2021.115337.

References

Adhikari, K., Hartemink, A.E., 2016. Linking soils to ecosystem services – a global review. Geoderma 262, 101–111.

Balco, G., Stone, J.O., Lifton, N.A., Dunai, T.J., 2008. A complete and easily accessible means of calculating surface exposure ages or erosion rates from ^{10}Be and ^{26}Al measurements. Quat. Geochronol. 3, 174–195.

Baude, M., Meyer, B.C., Schindewolf, M., 2019. Land use change in an agricultural landscape causing degradation of soil based ecosystem services. Sci. Total Environ. 659, 1526–1536.

Benton, M.J., Cook, E., Turner, P., 2002. Permian and Triassic Red Beds and the Penarth Group of Great Britain. Joint Nature Conservation Committee, Peterborough.

Bloch, S., Lander, R.H., Bonnell, L., 2002. Anomalously high porosity and permeability in deeply buried sandstone reservoirs: Origin and predictability. Am. Assoc. Pet. Geol. Bull. 86 (2), 301–328.

Bloomfield, J.P., Moreau, M.F., Newell, A.J., 2006. Characterization of permeability distribution in six lithofacies from the Helsby and Wilmslow sandstone formations of the Cheshire Basin, UK. In: Barker, R.D., Tellam, J.H. (Eds.), Fluid Flow and Solute Movement in Sandstones: The Onshore UK Permo-Triassic Red Bed Sequence. Geological Society, London, pp. 83–101.

Blum, W.E.H., 2005. Functions of Soil for Society and the Environment. Rev. Environ. Sci. Bio/Technol. 4, 75–79.

Borchers, B., Marrero, S., Balco, G., Caffee, M., Goehring, B., Lifton, N., Nishiizumi, K., Phillips, F., Schaefer, J., Stone, J., 2016. Geological calibration of spallation production rates in the CRONUS-Earth project. Quat. Geochronol. 31, 188–198.

Bowen, D.Q., Phillips, F.M., McCabe, A.M., Knutz, P.C., Sykes, G.A., 2002. New data for the Last Glacial Maximum in Great Britain and Ireland. Quat. Sci. Rev. 21, 89–101.

British Geological Survey, 2020. The BGS Lexicon of Named Rock Units – Bridgnorth Sandstone Formation. Available at: https://www.bgs.ac.uk/lexicon/lexicon.cfm?pub=BRI (Accessed: 7 February 2020).

Burley, S.D., 1984. 'Patterns of diagenesis in the Sherwood Sandstone Group (Triassic), United Kingdom'. Clay Minerals, 19, pp. 403–440.

Catt, J.A., King, D.W., Weir, A.H., 1975. The Soils of Woburn Experimental Farm I. Great Hill, Road Piece and Butt Close. Available at: http://www.era.rothamsted.ac.uk/eradoc/article/ResReport1974p2-5-30 (Accessed: 10 January 2020).

Cockburn, H.A.P., Summerfield, M.A., 2004. Geomorphological applications of cosmogenic isotope analysis. Progr. Phys. Geogr.: Earth Environ. 28 (1), 1–42.

Corbett, L.B., Bierman, P., Rood, D.H., 2016. An approach for optimizing in situ cosmogenic ^{10}Be sample preparation. Quat. Geochronol. 33, 24–34.

Cummins, W.A., 1962. The Greywacke problem. Geol. J. 3, 51–72.

Dietrich, W.E., Reiss, R., Hsu, M., Montgomery, D.R., 1995. A process-based model for colluvial soil depth and shallow landsliding using digital elevation data. Hydrol. Process. 9, 383–400.

Dobereiner, L., 1984. Engineering Geology of Weak Sandstones. PhD thesis. University of London. Available at: https://ethos.bl.uk/OrderDetails.do?uin=uk.bl.ethos.282418 (Accessed: 12 April 2020).

Dokuchaev, V.V., 1879. Mapping the Russian Soils. Imperial University of St. Petersburg, Russia.

Downing, R.A., Edmunds, W.M., Gale, I.N., 1987. Regional groundwater flow in sedimentary basins in the U.K. In: Goff, J.C., Williams, B.P.J. (Eds.), Fluid Flow in Sedimentary Basins and Aquifers. Geological Society of London, London, pp. 105–125.

Dyke, C.G., Dobereiner, L., 1991. Evaluating the strength and deformability of sandstones. Quarter. J. Eng. Geol. Hydrogeol. 24, 123–134.

Egli, M., Dahms, D., Norton, K., 2014. Soil formation rates on silicate parent material in alpine environments: different approaches-different results? Geoderma 213, 320–333.

Egli, M., Hunt, A.G., Dahms, D., Raab, G., Derungs, C., Raimondi, S., Yu, F., 2018. Prediction of Soil Formation as a Function of Age Using the Percolation Theory Approach. Front. Environ. Sci. 6 (108) https://doi.org/10.3389/fenvs.2018.00108.

Evans, D.J.A., Clark, C.D., Mitchell, W., 2005. The last British Ice Sheet: A review of the evidence utilised in the compilation of the Glacial Map of Britain. Earth Sci. Rev. 70 (3), 253–312.

Evans, D.L., Quinton, J.N., Tye, A.M., Rodés, Á., Davies, J.A.C., Mudd, S.M., Quine, T.A., 2019. Arable soil formation and erosion: a hillslope-based cosmogenic nuclide study in the United Kingdom. Soil 5, 253–263. https://doi.org/10.5194/soil-5-253-2019.

Evans, D., Rodés, A., Tye, A.M., 2020a. The Sensitivity of Cosmogenic Radionuclide Analysis to Soil Bulk Density: Implications for Soil Formation Rates. Eur. J. Soil Sci. doi: 10.1111/ejss.12982.

Evans, D.L., Quinton, J.N., Davies, J.A.C., Zhao, J., Govers, G., 2020b. Soil lifespans and how they can be extended by land use and management change. Environ. Res. Lett. 15(9). doi: 10.1088/1748-9326/aba2fd.

Eyers, J., 1991. The influence of tectonics on early Cretaceous sedimentation in Bedfordshire, England. J. Geol. Soc. 148, 405–414.

Eyles, N., McCabe, A.M., Bowen, D.Q., 1994. 'The stratigraphic and sedimentological significance of late Devensian ice sheet surging in Holderness, Yorkshire, UK. Quarter. Sci. Rev. 13, 727–759.

FAO, 2015. Status of the World's Soil Resources (SWSR) Main Report, Food and Agriculture Organisation of the United Nations and Intergovernmental Technical Panel on Soils, Rome, Italy.

Fifield, L.K., 1999. Accelerator mass spectrometry and its application. Rep. Prog. Phys. 62, 1223–1274.

Fullen, M.A., 1985. Erosion of arable soils in Britain. Int. J. Environ. Stud. 26, 55–69.

Fullen, M.A., 1991. Soil organic matter and erosion processes on arable loamy sand soils in the west midlands of England. Soil Technol. 4 (1), 19–31.

Fullen, M.A., 1992. Erosion rates on bare loamy sand soils in East Shropshire, UK. Soil Use Manag. 8, 157–162.

Fullen, M. A. (2020) Email to Dan Evans, 10 February.

Gibbard, P.L., Clark, C.D., 2011. Pleistocene Glaciation Limits in Great Britain. In: Ehlers, J., Gibbard, P.L., Hughes, P.D. (Eds.), Quaternary Glaciations –Extent and Chronology: a closer look. Elsevier, Amsterdam, pp. 75–93.

Gontier, A., Rihs, S., Chabaux, F., Lemarchand, D., Pelt, E., Tarpault, M., 2015. Lack of bedrock grain size influence on the soil production rate. Geochim. Cosmochim. Acta 166, 146–164.

Heimsath, A.M., Whipple, K.X., 2019. Strength matters: resisting erosion across upland landscapes. Earth Surf. Proc. Land. 44, 1748–1754.

Heimsath, A.M., Dietrich, W.E., Nishiizumi, K., Finkal, R.C., 1997. The Soil Production Function and Landscape Equilibrium. Nature 388, 358–361.

Heimsath, A.M., Dietrich, W.E., Nishiizumi, K., Finkel, R.C., 2001. Stochastic processes of soil production and transport: erosion rates, topographic variation and cosmogenic nuclides in the Oregon Coast Range. Earth Surf. Proc. Land. 26, 531–532.

Hollis, J.M., Reed, A.H., 1981. The Pleistocene deposits of the southern Worfe catchment. Proc. Geologists' Assoc. 92, 59–74.

Huggett, J.M., 1982. The growth and origin of authigenic clay minerals in sandstones. PhD thesis. University of London. Available at: https://spiral.imperial.ac.uk/handle/10044/1/35945 (Accessed: 13 September 2020).

Hunt, A.G., Ghanbarian, B., 2016. Percolation theory for solute transport in porous media: Geochemistry, geomorphology, and carbon cycling. Water Resour. Res. 52 (9), 7444–7459.

IUSS Working Group WRB: World Reference Base for Soil Resources 2014, update 2015 International soil classification system for naming soils and creating legends for soil maps, World Soil Resources Reports No. 106, FAO, Rome, 2015.

Jenny, H., 1941. Factors of Soil Formation: A System of Quantitative Pedology. McGraw-Hill, New York.

Kohl, C.P., Nishiizumi, K., 1992. Chemical isolation of quartz for measurement of in-situ produced cosmogenic nuclides. Geochim. Cosmochim. Ac. 56, 3583–3587.

Lal, D., 1991. Cosmic ray labelling of erosion surfaces: in situ nuclide production rates and erosion models. Earth Planet. Sc. Lett. 104, 424–439.

Matlack, K.S., Houseknecht, D.W., Applin, K.R., 1989. Emplacement of clay into sand by infiltration. J. Sediment. Res. 59 (1), 77–87.

McBratney, A., Field, D.J., Koch, A., 2014. The dimensions of soil security. Geoderma 212, 203–213.

Minasny, B., McBratney, A.B., 1999. A rudimentary mechanistic model for soil production and landscape development. Geoderma 90, 3–21.

Minasny, B., Finke, P., Stockmann, U., Vanwalleghem, T., Bratney, A.B., 2015. Resolving the integral connection between pedogenesis and landscape evolution. Earth-Sci. Rev. 150, 102–120.

Montgomery, D.R., 2007. Soil erosion and agricultural sustainability. P. Natl. Acad. Sci. USA 104, 13268–13272.

Morel, P., von Blankenburg, F., Schaller, M., Kubik, P.W., Hinderer, M., 2003. 'Lithology landscape dissection and glaciation controls on catchment erosion as determined by cosmogenic nuclides in river sediment (the Wutach Gorge, Black Forest). Terra Nova 15, 398–404.

Mountney, N.P., Thompson, D.B., 2002. 'Stratigraphic evolution and preservation of aeolian dune and damp/wet interdune strata: an example from the Triassic Helsby Sandstone Formation, Cheshire Basin, UK. Sedimentology 49, 805–833.

Owen, H.G., 1992. The Gault-Lower Greensand Junction Beds in the northern Weald (England) and Wissant (France), and their depositional environment. Proc. Geologists' Assoc. 103, 83–110.

Palmer, S.N., Barton, M.E., 1987. Porosity reduction, microfabric and resultant lithification in UK uncemented sands. In: Marshall, J.D. (Ed.), Diagenesis of Sedimentary Sequences. Geological Society, London, pp. 29–40.

Palumbo, L., Hetzel, R., Tao, M., Li, X., 2009. Topographic and lithologic control on catchment-wide denudation rates derived from cosmogenic ^{10}Be in two mountain ranges at the margin of NE Tibet. Geomorphology 117, 130–142.

Panagos, P., Borelli, P., Meusburger, K., Alewell, C., Lugato, E., Montanarella, L., 2015. Estimating the soil erosion cover- management factors at the European scale. Land Use Policy 48, 38–50.

Pettijohn, F.J., Potter, P.E., Siever, R., 1987. Sand and Sandstone. Springer-Verlag, New York.

Phillips, F.M., Argento, D.C., Balco, G., Caffee, M.W., Clem, J., Dunai, T.J., Finkel, R., Goehring, B., Gosse, J.C., Hudson, A.M., Jull, A.J.T., Kelly, M.A., Kurz, M., Lal, D., Lifton, N., Marrero, S.M., Nishiizumi, K., Reedy, R.C., Schaefer, J., Stone, J.O.H., Swanson, T., Zreda, M.G., 2016. The CRONUS-Earth Project: A synthesis. Quat. Geochronol. 31, 119–154.

Pimentel, D., Harvey, C., Resosudarmo, P., Sinclair, K., Kurz, D., McNair, M., Crist, S., Shpritz, L., Fitton, L., Saffouri, R., Blair, R., 1995. Environmental and Economic Costs of Soil Erosion and Conservation Benefits. Science 267, 1117–1123.

Portenga, E.W., Bierman, P.R., 2011. Understanding Earth's eroding surface with ^{10}Be. GSA Today 21, 4–10.
Quinton, J.N., Catt, J.A., 2004. 'The effects of minimal tillage and contour cultivation on surface runoff, soil loss and crop yield in the long-term Woburn Erosion Reference Experiment on sandy soil at Woburn, England '. Soil Use Manag. 20 (3), 343–350.
Quinton, J.N., Govers, G., Van Oost, K., Bardgett, R.D., 2010. The impact of agricultural soil erosion on biogeochemical cycling. Nat. Geosci. 3, 311–314.
Radley, J.D., Coram, R.A., 2016. The Chester Formation (Early Triassic, southern Britain): sedimentary response to extreme greenhouse climate. Proc. Geologists' Assoc. 127 (5), 552–557.
Rastall, R.H., 1919. The Mineral Composition of the Lower Greensand Strata of Eastern England. Geol. Mag. 6 (5), 211–220.
Reed, A.H., 1979. Accelerated erosion of arable soils in the United Kingdom by rainfall and runoff. Outlook Agric. 10 (1), 41–48.
Rodés, Á., Evans, D.L., 2019. Cosmogenic soil production rate calculator. MethodsX 7, 1–5.
Shotton, F.W., 1967. Age of the Irish Sea Glaciation of the Midlands. Nature 215, 1366.
Simonson, R.W., 1997. Early Teaching in USA of Dokuchaiev Factors of Soil Formation. Soil Sci. Soc. Am. J. 61 (1), 11–16.
Stark, T.D., Eid, H.T., 1994. Drained residual strength of cohesive soils. J. Geotech. Eng. 120 (5), 856–871.
Stead, D., Eyers, J., 2017. The palynology and geology of the Lower Cretaceous (Aptian-Albian) of Munday's Hill Quarry, Bedfordshire, UK. Proc. Geologists' Assoc. 128 (4), 599–612.
Stockmann, U., Minasny, B., McBratney, A.B., 2014. How fast does soil grow? Geoderma 216, 48–61.
Stride, A.H., 1982. Offshore tidal sands: Processes and deposits. Chapman and Hall, London.
Strong, G.E., 1993. Diagenesis of Triassic Sherwood Sandston Group rocks, Preston, Lancashire, UK: a possible evaporitic cement precursor to secondary porosity? In: North, C.P., Prosser, D.J. (Eds.), Characterization of Fluvial and Aeolian Reservoirs. Geological Society, London, pp. 279–289.
Targulian, V.O., Krasilnikov, P.V., 2007. Soil system and pedogenic processes: Self-organization, time scales, and environmental significance. Catena 71 (3), 373–381.
Tellam, J.H., 1995. 'Hydrochemistry of the saline groundwaters of the lower Mersey Basin Permo-Triassic sandstone aquifer, UK. J. Hydrol. 165, 45–84.
Tye, A.M., Kemp, S.J., Lark, R.M., Milodowski, A.E., 2012. The role of peri-glacial active layer development in determining soil-regolith thickness across a Triassic sandstone outcrop in the UK. Earth Surf. Proc. Land. 37, 971–983.
Watson, E., Morgan, A., 1977. The Periglacial Environment of Great Britain during the Devensian [and Discussion]. Philos. Trans. Royal Soc. London B Biol. Sci. 280, 183–198.
Wakatsuki, T., Tanaka, Y., Matsukura, Y., 2005. Soil slips on weathering-limited slopes underlain by coarse-grained granite or fine-grained gneiss near Seoul, Republic of Korea. Catena 60 (2), 181–203.
Walker, T.R., Waugh, B., Crone, A.J., 1978. Diagenesis in first cycle desert alluvium of Cenozoic age, southwestern United States and northwestern Mexico. Geol. Soc. Am. Bull. 89, 19–32.
Wilkinson, M.T., Humphreys, G.S., 2005. Exploring pedogenesis via nuclide-based soil production rates and OSL-based bioturbation rates. Aust. J. Soil Res. 43, 767–779.
Wilkinson, M.T., Chappell, J., Humphreys, G.S., Fifield, K., Smith, B., Hesse, P., Heimsath, A.M., Ehlers, T.A., 2005. Soil production in heath and forest, Blue Mountains, Australia: influence of lithology and palaeoclimate. Earth Surf. Proc. Land. 30, 923–934.
Xu, S., Dougans, A.B., Freeman, S., Schnabel, C., Wilcken, K.M., 2010. Improved Be-10 and Al-26 AMS with a 5 MV spectrometer, in: Nuclear Instruments and Methods in Physics Research Section B: Beam Interactions with Materials and Atoms, Eleventh International Conference on Accelerator Mass Spectrometry, Rome, Italy, 14–19 September 2008, 736–738.